THE ASTROPHYSICAL JOURNAL, 475:L41–L44, 1997 January 20

ON PROTOSTELLAR DISKS IN HERBIG Ae/Be STARS

ANATOLY MIROSHNICHENKO,[1] ŽELJKO IVEZIĆ,[2] AND MOSHE ELITZUR[3]
Department of Physics and Astronomy, University of Kentucky, Lexington, KY 40506-0055
Received 1996 July 17; accepted 1996 November 5

ABSTRACT

The spectral shape of IR emission from Herbig Ae/Be stars has been invoked as evidence for accretion disks around high-mass protostars. Instead, we present here models based on spherical envelopes with an $r^{-1.5}$ dust density profile that successfully explain the observed spectral shapes. The spectral energy distributions of eight primary candidates for protostellar disks are fitted in detail for all wavelengths available, from visual to far-IR. The only envelope property adjusted in individual sources is the overall visual optical depth, and it ranges from 0.3 to 3. In each case, our models properly reproduce the data for IR excess, visual extinction, and reddening. The success of our models shows that accretion disks cannot make a significant contribution to the radiation observed in these pre–main-sequence stars.

Subject headings: accretion, accretion disks — circumstellar matter — dust, extinction — stars: pre–main-sequence

1. INTRODUCTION

Disks are expected to form during protostellar collapse, and low-mass stars seem to provide good observational evidence for the existence of disks—a large body of T Tauri observations is successfully integrated in a model based on circumstellar disks (Bertout & Basri 1991). On the other hand, in high-mass stars, which form under different conditions with a strong tendency to cluster, the observational evidence for disks is less compelling. Based on the spectral energy distributions (SEDs) of a sample of 47 Herbig Ae/Be stars, the high-mass ($\gtrsim$1.5 $M_\odot$) counterparts of T Tauri stars, Hillenbrand et al. (1992, hereafter HSVK) proposed that most of these objects also are surrounded by massive accretion disks. The SEDs were classified into three groups, and HSVK suggested that the IR emission from the 30 objects in group I is generated purely in optically thick accretion disks. However, this proposal encountered some serious difficulties, summarized by Evans & Di Francesco (1995). In particular, from far-IR imaging of group I sources Di Francesco et al. (1994) conclude that optically thick disks cannot account for the observed far-IR emission and that another component is required, most likely a circumstellar envelope.

HSVK invoked the IR spectral behavior $\lambda F_\lambda \propto \lambda^{-4/3}$ as the primary signature of optically thick disks. However, the emission from a spherical envelope with the density law $\rho(r) \propto r^{-p}$ obeys $\lambda F_\lambda \propto \lambda^{-(p-1)(\beta+4)/2}$ if the envelope is optically thin in the wavelength regime where the opacity varies according to $\kappa_\lambda \propto \lambda^{-\beta}$ (Harvey et al. 1991). Interstellar grains have $\beta = 1$–2 at IR wavelengths; thus, the $\lambda F_\lambda \propto \lambda^{-4/3}$ behavior is reproduced with $p \sim 1.5$, the expected spectral index of the density profile during the spherical collapse phase (e.g., Shu, Adams, & Lizano 1987). Indeed, Hartmann, Kenyon, & Calvet (1993, hereafter HKC) produced models for spherical envelopes with an $r^{-1.5}$ density profile that closely resemble the observed SEDs of Ae/Be stars longward of approximately 3 μm. But the flux emerging in the visible region was too small in these models, and HKC suggested that there is a clear line of sight to the star through the envelope, perhaps cleared by bipolar outflows. The large axial cavities required by this proposal somewhat blur the distinction between disk and spherical geometries.

A prerequisite for settling this important controversy is a definitive answer to the following question: are spherical distributions at all capable of producing the observed SEDs of Herbig Ae/Be stars? And if they are, what is the minimal set of independent parameters that would have to be adjusted in fitting each individual source? In this Letter we attempt to answer these questions. Rowan-Robinson (1980) was the first to show that IR emission from spherical shells possesses general scaling properties. This result was recently extended to arbitrary systems—for any type of geometry and density distribution, infrared emission from radiatively heated dust possesses general scaling properties when the region's inner boundary is controlled by dust sublimation (Ivezić & Elitzur 1996, hereafter IE96). Thanks to scaling, the number of free parameters is greatly reduced, enabling a systematic study of the spectral properties that can and cannot be produced by any family of models. Here we utilize the scaling approach for detailed modeling of the SEDs observed in Herbig Ae/Be stars.

2. MODELING

We have developed a numerical code, described in IE96, that solves exactly the radiative transfer spherical problem taking full advantage of scaling. Only two scales need be specified for a complete solution when the shell's inner radius is controlled by dust sublimation—the sublimation temperature $T_{\rm sub}$ and the overall optical depth at some fiducial, arbitrary wavelength. For simplicity, we choose $T_{\rm sub} = 1500$ K in all sources for both graphite and silicate grains. The small differences that may exist between these species, as well as variations of $T_{\rm sub}$ itself, have a negligible effect on the results. We choose 0.55 μm as the fiducial wavelength that sets the scale of optical depth, and the corresponding τ_V is the only free parameter allowed to be adjusted in modeling of individual sources. All other input properties involve dimensionless, normalized profiles that fall into three categories:

[1] Permanent address: Pulkovo Observatory, St. Petersburg 196140, Russia; anat@pulkovo.spb.su.
[2] ivezic@pa.uky.edu.
[3] moshe@pa.uky.edu.

TABLE 1

PROPERTIES OF MODELED STARS

IRAS Number (1)	Name (2)	Type (3)	V (4)	τ_{V0} (5)	A_V (6)	τ_V (7)
00403+6138	BD +61°154	B8	10.55	2.7	0.7	1.8
04555+2946	HD 31648	A2	7.66	0.4	…	…
05385−0244	HD 37806	B9	7.95	0.7	…	…
11575−7754	HD 104237	A4	6.60	0.5	…	…
16372−2347	HD 150193	A1	8.55	1.6	1.4	0.3
17070−2711	KK Oph	A5	9.40	1.7	0.4	1.2
19238+2106	WW Vul	A3	10.30	1.0	…	…
20005+0535	HD 190073	A0	7.87	0.5	…	…

NOTE.—Col. (1), IRAS number; col. (2), other name of modeled stars; col. (3), spectral type; col. (4), observed visual magnitude; col. (5), visual optical depth of the circumstellar dust shell obtained from the model fit to the data without any correction for interstellar extinction; col. (7), interstellar extinction; col. (8), optical depth when dereddening the data improves the overall fit.

1. *The external radiation.*—Luminosity is irrelevant. The normalized profile F_λ/F, where F is bolometric flux, is the only input required for the external radiation. For each source we use the spectral shape of the Kurucz (1979) model atmosphere corresponding to the spectral type of the central star.

2. *Dust optical properties.*—The magnitude of the absorption coefficient is irrelevant, only the extinction spectral shape $q_\lambda = \kappa_\lambda/\kappa_V$ and albedo ϖ_λ enter. These quantities are determined by the grain chemical composition and size distribution, and we assume that both properties are uniform throughout the envelope. Following Draine & Lee (1984), the chemical composition is a mixture of astronomical silicate and graphite grains at the ratio $n_{\rm Si}:n_{\rm C} = 1.12$. We take the graphite dielectric coefficient from Draine & Lee, and the silicate from the more recent study by Ossenkopf, Henning, & Mathis (1992). The size distribution is the one proposed by Mathis, Rumpl, & Nordsieck (1977, hereafter MRN) in which grain radii obey $a \gtrsim a_- = 0.005$ μm and $a \lesssim a_+ = 0.25$ μm.

3. *Dust density distribution.*—The density scale is irrelevant, as is the size scale of all geometrical dimensions; both enter as one independent parameter, the overall optical depth. Only the spatial distribution of dust, described by a dimensionless, normalized distribution, is required. We introduce the dimensionless radial coordinate $y = r/r_1$, where r_1 is the dust sublimation radius. The shell inner boundary is always at $y = 1$, and the actual value of r_1 never enters. If the dust density is denoted $\rho_d(r)$, only the dimensionless, normalized distribution $\eta(y) = \rho_d(y)/\int_1^\infty \rho_d(y)\, dy$ is required. We choose $\eta \propto y^{-1.5}$, attempting to model all sources with a single density profile.

2.1. *Data*

In the recent catalog of Thé, Pérez, & de Winter (1994) we have identified all the Herbig Ae/Be stars with good spectral coverage from 0.3 μm to far-IR wavelengths, including IRAS data of reliable quality; in some cases we improved on the listing in the IRAS point-source catalog using the ADDSCAN procedure (Weaver & Jones 1992). Among these sources we looked for those that meet the HSVK disk criterion $\lambda F_\lambda \propto \lambda^{-4/3}$ for the underlying continuum to the longest wavelength observed. We then selected for detailed modeling those stars that show evidence for the 10 μm silicate feature commensurate with the standard $n_{\rm Si}:n_{\rm C}$ ratio used here. The eight sources listed in Table 1, with spectral types from Thé et al. (1994), meet all of these selection criteria and were used in the modeling presented here. A future detailed paper will present models for additional objects, including carbon-rich shells.

Herbig Ae/Be stars show considerable variability. We have carefully studied all available data pertaining to the light curves of our sources, including data from the recent long-term optical monitoring programs of Manfroid et al. (1991) and Shevchenko et al. (1993). The reddening some Ae/Be stars exhibit at visual wavelengths during brightness decreases is attributed to occultation by optically thick dust clumps in their envelopes (e.g., Grinin et al. 1991). Two of the sources selected for fitting (KK Oph, WW Vul) display such variability, and in each case we choose the observations at maximum visual brightness. Other sources are not known as highly variable stars, and we simply average their photometric data. In most cases optical and IR observations are nonsimultaneous; for each source we tried to choose data as contemporaneous as possible.

3. RESULTS

Extinction of the stellar radiation is caused both by foreground interstellar material and the circumstellar shell, and normally it is impossible to distinguish between the two; correction for interstellar reddening cannot be performed when the shell effect is not known, and a model cannot be fitted without reddening-corrected data. Indeed, the procedure used by HSVK to estimate the interstellar extinction A_V simply ignored the effect of the circumstellar matter on $B - V$. However, within the context of a model for the shell, the two components can be disentangled with the aid of an additional color excess that is affected also by dust emission. This emission comes only from the shell[4] and is significant only for $\lambda \gtrsim 2$–3 μm, since shorter wavelengths require dust hotter than the sublimation temperature. In Figure 1 we show the data points in a diagram of the color excesses over the naked star spectrum for $B - V$ and $V - [12]$, where [12] is the 12 μm magnitude. Corrections for interstellar reddening would move data points to the left parallel to the dotted line by distances proportional to the corresponding A_V value. Our models produce a track in this diagram, drawn with a solid line, originating from the naked star location (0, 0), with distance along the track increasing with τ_V. In the absence of interstellar extinction, data points would lie on this line, and their

[4] Interstellar dust emission (cirrus) can affect only $\lambda \gtrsim 60$ μm in some sources.

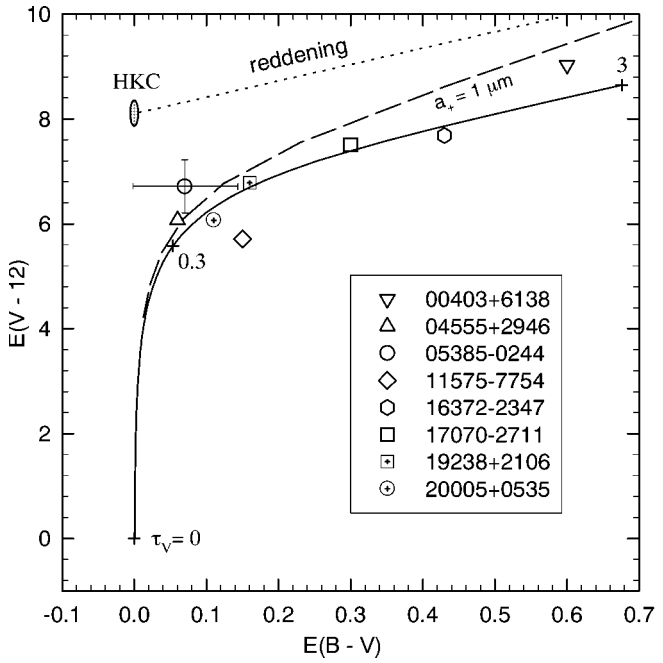

FIG. 1.—Color excess diagram for the stars in our sample. $E(B - V)$ is affected only by the combined effect of interstellar and circumstellar extinction, while $E(V - 12)$ is affected also by circumstellar dust emission. Data points are denoted by the symbols listed in the legend. Error bars shown for IRAS 05385−0244 are common to all stars. Corrections for interstellar reddening would move each data point to the left parallel to the dotted line marked "reddening" by a distance proportional to the corresponding A_V. The ellipse marked HKC is the prediction of the Hartmann et al. (1993) model for cavity opening angles ranging from 30° to 60°. The solid line is the prediction of our model with MRN dust composition. Position along this line is determined by the dust shell optical depth τ_V, with $\tau_V = 0$ (a naked star), 0.3, and 3 marked by crosses. The dashed line is our model result when the upper limit of the grain size distribution is increased from 0.25 to 1 μm.

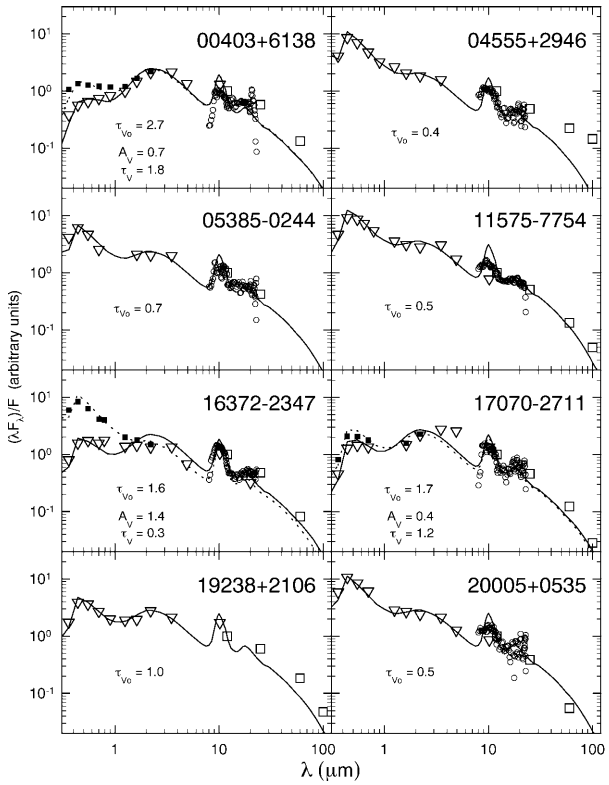

FIG. 2.—Observations and model results for the eight stars listed in Table 1. Each panel is identified by the source IRAS number. IRAS data are denoted by circles and open squares for the LRS and PSC listings, respectively. Triangles denote all other data without any correction for interstellar extinction. This correction is important only for $\lambda \leq 2.2$ μm, and the full squares in some panels are the same data corrected for extinction with the listed A_V values. The lines are the results of detailed numerical calculations with the model described in the text. The only envelope parameter allowed to vary is the optical depth, denoted in each panel. Full lines correspond to the optical depth τ_{V0}, dotted lines to τ_V.

positions would determine the optical depth of each shell. The fact that within errors all the data points do indeed lie on the displayed track supports our model and indicates that A_V could be negligible for all members of this sample. Furthermore, Figure 2 shows the spectra calculated for the optical depths τ_{V0} determined for each source from its location, within the errors, on the track of Figure 1. These models produce satisfactory fits for the raw data without any correction for interstellar reddening over the entire spectral range, not just the three wavelengths used for the determination of τ_{V0}. This detailed agreement provides further support for our model.

The large observational error bars and the similar slopes of the reddening line and our model track for $E(B - V) \gtrsim 0.1$ introduce ambiguities into the determination of τ_V and A_V. For three sources, reddening corrections performed within the bounds of these ambiguities result in equal or better fits, also presented in Figure 2; in the case of IRAS 16372−2347, this model noticeably improves the fit around 2–5 μm. In each case, the spectral shapes of the two models are identical for $\lambda \gtrsim 5$ μm because the shells are optically thin at these wavelengths. Table 1 lists the optical depths τ_{V0} for all sources, and A_V and τ_V values for the three sources whose shell properties remain slightly ambiguous.

Our models provide some constraints on the dust properties. The sublimation temperature can be varied by a few hundred degrees around 1500 K with little change in the models. The only minor effect is a slight shift in the wavelength of the emission peak discernible around 2–3 μm. In the case of KK Oph, this shift improves the fit for $T_{sub} \simeq 1000$ K. The dust chemistry is primarily constrained by the strength of the 10 μm feature. For all the sources displayed here, n_{Si}:n_C can vary from its standard value by no more then approximately 20% in either direction. It should be noted, however, that other sources, which we will analyze in a future detailed paper, give clear evidence for carbon-rich dust. A primary example is HR 5999, as noted already by Thé et al. (1996). Grain sizes are primarily constrained by $U - B - V$ and $K - [12]$ colors. We find that the distribution upper limit a_+ must fall in the range 0.2–1 μm for these sources, and we present in Figure 1 the model track when a_+ is increased to its maximum allowed value of 1 μm. The lower limit must obey $a_- \lesssim 0.05$. Both limits are consistent with the MRN estimates for interstellar grains.

The spectral index of the dust density profile used in all our models is $p = 1.5$, as expected in free-fall accretion. Satisfactory fits are produced only in the rather narrow range $p \simeq 1.4$–1.6. At lower values of p the near-IR bump is overly suppressed, whereas at larger p the far-IR radiation is overly suppressed. However, there are Herbig Ae/Be stars that show strong evidence for other density profiles, which we will present separately, presumably reflecting different evolutionary stages.

4. DISCUSSION

Our model results, shown in Figure 2, answer the questions posed in the Introduction. The SEDs of these sources, primary examples of accretion disks according to HSVK, are successfully modeled with spherical envelopes that differ from each other in only one property: the optical depth τ_V, listed in each panel and in Table 1. Furthermore, since these SEDs display the 10 μm feature in emission, they *cannot* be produced by optically thick accretion disks. Irrespective of geometry, an emission feature is never produced if the source is optically thick in the corresponding wavelength regime. By contrast, the 10 μm optical depths of our spherical models vary from 0.01 to 0.1.

Because of the inherent scaling properties of the radiative transfer problem, modeling can determine τ_V but can never provide information on density scale or physical dimensions. These quantities can be estimated only if additional information is provided. For luminosity L in solar units, $r_1 \sim 10^{12} L^{1/2}$ cm (IE96). The 100 μm radiation originates from regions where the dust temperature is approximately 40 K, corresponding to $r \sim 10^4\, r_1$. Therefore, a stellar luminosity of order 100 $L_\odot$ will result in shell sizes of order 10^4 AU at 100 μm, as observed (e.g., Di Francesco et al.). With standard gas-to-dust mass ratio $r_{gd} = 200$, the gas column density outside the sublimation radius r_1 is $(2 \times 10^{21})\tau_V$ cm^{-2}. For free-fall accretion, this column corresponds to $\dot{M} = (0.5 \times 10^{-8})\tau_V M^{1/2} L^{1/4}$ $M_\odot$ yr^{-1}, where M is the central mass in solar units. It should be noted that if grains are depleted in the envelope, then r_{gd} increases, and with it the estimate of $\dot{M}$.

Our model envelopes are purely spherical. By contrast, HKC invoke large axial cavities in their spherical configurations even though they too attribute the IR emission to $r^{-3/2}$ density distribution. HKC present two detailed model calculations. The one relevant for the sources considered here, because it displays the 10 μm feature in emission, has $\dot{M} = 10^{-6}\, M_\odot$ yr^{-1}, corresponding to $\tau_V = 30$–40; our calculations with such τ_V reproduce the SED presented by HKC. Because of the large extinction of this model, the stellar radiation is heavily extinguished by the envelope. To produce the observed visual fluxes, HKC proposed axial cavities as a means to obtain a clear line of sight to the star, so that in this scheme, the observed $E(B - V)$ is determined purely by interstellar extinction. The ellipse marked HKC in Figure 1 shows their model predictions, and all data points should congregate on the reddening line originating from it. Instead, all the sources in our sample fall below this line, more than 2 standard deviations away. If A_V is determined from $E(B - V)$, then the HKC model predictions exceed the observed 12 μm flux by more than 2 mag. One could attempt to modify the HKC approach with grazing rays, producing a partially obscured star, but this only exacerbates the problem because then the HKC ellipse moves upward and to the right in the diagram, away from the data points. The HKC model is not adequate for the sources in this sample because its optical depth is so large. If there is no dust depletion in these shells, the smaller optical depths required by the data imply mass loss rates 10–100 times smaller than those employed by HKC.

In conclusion, our study amplifies the findings by Di Francesco et al. (1994) that extended envelopes, optically thin at IR wavelengths, dominate the IR emission from group I Herbig Ae/Be stars. If present, optically thick accretion disks can only make a negligible contribution to the observed radiation. Large axial cavities are not present in the sources modeled here. Similarly, free-free emission by circumstellar gas, advocated by Berrilli et al. (1992), seems to be superfluous.

We are grateful for the permission to use unpublished photometric data by V. S. Shevchenko and W. Wenzel. Our model fitting procedure was greatly aided by a program developed by Charles Danforth. We thank the Center for Computational Sciences at the University of Kentucky, especially the director John Connolly, for generous support that made this collaboration possible. Support by the Exchange of Astronomers Program of the IAU (A. M.), NSF grant AST-9321847, and NASA grant NAG 5-3010 is gratefully acknowledged.

REFERENCES

Berrilli, F., et al. 1992, ApJ, 398, 254
Bertout, C., & Basri, G. 1991, in The Physics of Star Formation and Early Stellar Evolution, ed. C. J. Lada & N. D. Kylafis (Dordrecht: Kluwer), 649
Di Francesco, J., Evans, N. J., II, Harvey, P. M., Mundy, L. G., & Butner, H. M. 1994, ApJ, 432, 710
Draine, B., & Lee, H. M. 1984, ApJ, 285, 89
Evans, N. J., II, & Di Francesco, J. 1995, Rev. Mexicana Astron. Astrofis., 1, 187
Grinin, V. P., Kiselev, N. N., Chernova, G. P., Minikulov, N. Kh., & Voshchinnikov, N. V. 1991, Ap&SS, 186, 283
Hartmann, L., Kenyon, S. J., & Calvet, N. 1993, ApJ, 407, 219 (HKC)
Harvey, P. M., Lester, D. F., Brock, D., Joy, M. 1991, ApJ, 368, 558
Hillenbrand, L. A., Strom, S. E., Vrba, F. J., & Keene, J. 1992, ApJ, 397, 613 (HSVK)
Hillenbrand, L. A., Strom, S. E., Vrba, F. J., & Keene, J. 1996, MNRAS, submitted (IE96)
Kurucz, R. L. 1979, ApJS, 40, 1
Manfroid, J., et al. 1991, ESO Sci. Rep., No. 8
Mathis, J. S., Rumpl, W., & Nordsieck, K. H. 1977, ApJ, 217, 425 (MRN)
Ossenkopf, V., Henning, Th., & Mathis, J. S. 1992, A&A, 261, 567
Rowan-Robinson, M. 1980, ApJS, 44, 403
Shevchenko, V. S., Grankin, K. N., Ibragimov, M. A., Melnikov, S. Yu., & Yakubov, S. D. 1993, Ap&SS, 202, 121
Shu, F., Adams, F. C., & Lizano, S. 1987, ARA&A, 25,23
Thé, P. S., Pérez, M. R., & de Winter, D. 1994, A&AS, 104, 315
Thé, P. S., Pérez, M. R., Voshchinnikov, N. V., & van den Ancker, M. E. 1996, A&A, in press
Weaver, Wm. B., & Jones, G. 1992, ApJS, 78, 239